East European Journal of Physics. **4.** 357-369 (2025)
DOI:10.26565/2312-4334-2025-4-33 ISSN 2312-4334

IMPACT OF MAGNETIC FIELD ON PERISTALTIC TRANSPORT OF NANO-COUPLED STRESS FLUID IN AN INCLINED POROUS TUBE

M.P. Molimol[1,2], K. Maruthi Prasad[1]*, N. Subadra[2]
[1]*Department of Mathematics, School of Science, GITAM (Deemed to be University), Hyderabad, Telangana state, India -502329*
[2]*Department of Mathematics, Geethanjali College of Engineering and Technology, Medchal Dist., Hyderabad, Telangana state, India -501301*
**Corresponding Author e-mail: mkaranam@gitam.edu*
Received September 1, 2025; revised October 10, 2025; accepted October 18, 2025

This study provides a theoretical investigation of peristaltic transport of couple-stress nanofluid under the influence of a magnetic field in an inclined porous tube. With low Reynolds number, long wavelength approximations, appropriate analytical methods are employed to investigate the fluid's velocity, frictional force, time-averaged flux, nanoparticle phenomena, pressure drop, and temperature profile. The effects of various physical parameters, including the thermophoresis parameter, Brownian motion parameter, local nanoparticle Grashof number, and local temperature Grashof number, on frictional force and pressure drop characteristics are investigated. Graphs are used to illustrate expressions for pressure drop, velocity, nanoparticle phenomena, temperature profile, and frictional force.
Keywords: *Thermophoresis parameter; Peristalsis; Brownian motion parameter; Nanoparticles; Magnetic field; Couple stress fluid; Porous medium*
PACS: 47.15.-x, 47.63.-b, 47.50.-d

Nomenclature

a^*	'Tube Radius'	C'	'Nanoparticle Concentration'
b^*	'Amplitude'	${D_B}^*$	'Brownian diffusion coefficient'
c_1	'Wave Speed'	${D_{T'}}^*$	'Thermophoretic diffusion coefficient'
λ^*	'Wave Length'	C_0'	'Nanoparticle Concentration as $r^* \to h$'
$\emptyset$	'Inclination Angle'	T_0'	'Ambient Temperature as $r^* \to h$'
T_{ij}^A and T_{ij}	'Antisymmetric Tensor and Symmetric Tensor'	θ^*	'Temperature'
${w_i}^*$	'Velocity Vector	σ^*	'Concentration'
M_{ij}	'Couple-stress Tensor'	N_t^*	'Thermophoresis parameter'
μ_{ij}	'Deviatoric part of M_{ij}'	N_b^*	'Brownian motion parameter'
${\omega_{ij}}^*$	'Vorticity Vector'	G_r^*	'Local temperature Grashof number'
d_{ij}	'Symmetric part of Velocity Gradient'	B_r^*	'Local nanoparticle Grashof number'
η and $\bar{\alpha}$	'Couple-stress Fluid Parameters'	r^*	'Radial Coordinate'
p	'Pressure'	z	'Axial Coordinate'
${\rho^*}_f$	'Fluid Density'	w^*	'Axial Velocity'
${\rho^*}_p$	'Density of Particle'	k	'Porosity'
F	'Body Force'	δ_1	'Electrical Conductivity'
C	'Volumetric thermal expansion coefficient'	B_0	'Uniform Magnetic Field'
d/dt	'Material derivative'	M^*	'Hartmann Number'

INTRODUCTION

Peristaltic pumping is the gradual contraction of a tube along its length. The cross-sectional area subsequently changes. Peristalsis naturally takes place in various tubular organs within the human body. Peristaltic motion has been used in several industrial applications, such as the transport of sterile and hygienic fluids, blood pumps for the heart and lungs, and the handling of chemically aggressive fluids. Researchers have studied the peristaltic transport of both non-Newtonian and Newtonian fluids under a wide range of conditions, recognizing its significance.

[1] conducted detailed research on Magnetohydrodynamic flow of nano-coupled stress fluid in the tapered, non-uniform passage within a porous medium, considering velocity slip and convective boundaries. Their model integrates key physical influences such as nanoparticle dynamics (Brownian motion and thermophoresis), magnetic fields, and porous resistance. Numerical results reveal that stronger magnetic fields reduce axial velocity but improve heat transfer. The wall-slip and permeable medium significantly affect the flow and thermal behaviour. [2] explained the combined impact of magnetic field and heat transfer on peristaltic transport of couple-stress fluid through an inclined tube. Their model accounts for body forces, low Reynolds number, and long wavelength approximation due to inclination, along with temperature-dependent source terms. The results reveal that flow characteristics, including temperature gradients, pressure rise, and velocity profiles, are significantly affected by the interplay between magnetic damping, couple stress effects, and inclination angle.

Cite as: M.P. Molimol, K. Maruthi Prasad, N. Subadra, East Eur. J. Phys. 4, 357 (2025), https://doi.org/10.26565/2312-4334-2025-4-33

[3-4] explained the theoretical study of the peristaltic flow of couple stress fluid, including mass and heat transfer effects. This study assumes a low Reynolds number, long wavelength approximation, which allows analytical solutions. Key aspects investigated are velocity distribution, time-averaged flux, frictional force, mechanical efficiency, pressure-drop, nanoparticle behaviour, coefficients of heat and mass transport, and temperature profile. The influence of several physical parameters, such as Brownian motion, the couple stress fluid parameter, thermophoresis, nanoparticle, and temperature Grashof numbers, is thoroughly examined. and further it was studied with nanoparticles in an inclined tube by [5].

Researchers typically use the couple-stress fluid model because it is more mathematically simpler than other models. Blood, lubricants with electro-rheological suspensions, synthetic fluids, and high polymer-based additives exhibit couple-stress and rotation, unlike Newtonian fluids. The couple stress fluid model provides a better representation for these fluids. [6] Stokes developed couple-stress fluids in 1966. [7] developed a stress model of blood flow in the microcirculation. [8] conducted a study on peristaltic transport of couple-stress fluid, focusing on its relevance to hemodynamic applications. [9] explored how the boundary layer affects peristaltic flow of couple stress fluid. [10] demonstrated the hydromagnetic influence on inclined peristaltic flow of couple stress fluid.

Nanotechnology has significant impact on industry due to the distinctive physiochemical characteristics of nanoscale materials. Common base fluids used in nanofluid applications include oil, ethylene glycol, and water. Nanofluids are widely utilized in heat transfer processes, including those in fuel cells, microelectronics, hybrid engines, and pharmaceutical manufacturing. There is extensive literature available on nano fluids and their uses. [11] was the first to research nanofluids and further it was studied in an inclined tube by [12]. [13] carried out research concerning pool boiling behaviour of nanofluids in horizontally oriented narrow tubes. [14] studied peristaltic motion of third order nanofluids under mixed convection in the presence of an inclined magnetic field. [15-17] investigated the peristaltic flow of nanoparticle-laden micropolar fluid, taking into account heat and mass transfer effects in an inclined tube. Many ducts in the physiological system are inclined with the axis, rather than being horizontal. [18] explored the effect of slip conditions on the peristaltic transport of power-law fluid through the inclined tube.

In the previous literature, the researchers studied (i) peristaltic transport of Newtonian or micropolar fluids with MHD, (ii) peristaltic transport of a couple-stress fluid with MHD, but without nanoparticles, porous medium. In this work, we considered couple-stress fluid with nanoparticles in an inclined tube under the influence of MHD through porous medium. This comprehensive model is especially important for advanced applications such as biomedical engineering (magnetic targeting of drug carriers in porous tissues and blood flow under external magnetic fields), thermal management of electronics (cooling microchips using nanofluids in porous heat sinks with MHD flow control), and industrial processes (peristaltic pumping of complex fluids in chemical reactors with porous linings).

With all of the aforementioned in mind, the peristaltic flow of couple stress nanofluid within inclined tube was examined under the assumptions of low Reynolds number and long wavelength. Homotopy perturbation method (HPM) was employed to solve the coupled equations governing temperature profile and nanoparticle phenomena. Analytical solutions for nanoparticle phenomena, velocity, temperature profile, frictional force, and pressure drop were developed. Impact of various conditions on these flow parameters has been represented using graphs.

MATHEMATICAL FORMULATION

Peristaltic flow of an incompressible couple-stress nanofluid having a uniform cross-sectional radius a_1 in an inclined tube. A sinusoidal wave travels along the tube border with amplitude b^*, wavelength λ^*, speed c_1, and inclined tube angle is $\emptyset$.

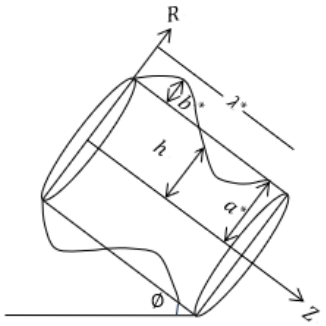

Figure 1. Geometry of the problem

Consider the cylindrical polar coordinate system (R, θ^*, Z) then the geometry of the wall surface is

$$R = H(z, t^*) = b^* Sin\frac{2\pi}{\lambda^*}(Z - c_1 t^*) + a^* \tag{1}$$

In a fixed coordinate frame, the governing equations of an incompressible couple-stress fluid containing nanoparticles, neglecting body couples or body moments, are expressed as follows

$$T_{ji.j} = \rho^* \frac{dw_i^*}{dt^*} \tag{2}$$

$$e_{ijk}{}^* T_{jk}^A + M_{ji.j} = 0 \tag{3}$$

$$l_{ij} = -p\delta_{ij}{}^* + 2\mu_{ij} d_{ij} \tag{4}$$

$$\mu_{ij} = 4\eta\omega_{j.i}{}^* + 4\eta'\omega_{ij}{}^* \tag{5}$$

$$(\rho^* c)_f \frac{dT'}{dt^*} = k\nabla^2 T' + (\rho^* c)_p \left[D_B{}^* \nabla C'.\nabla T' + \frac{D_{T'}{}^*}{T_0'} \nabla T'.\nabla T' \right] \tag{6}$$

$$\frac{dC'}{dt^*} = D_B{}^* \nabla^2 C' + \left[\frac{D_{T'}{}^*}{T_0'} \right] \nabla^2 T' \tag{7}$$

By applying the transformation

$$r^* = R, z = Z - c_1 t^*, \theta^* = \theta^*, u^* = U,\ w^* = W - c_1$$

Transforming from a stationary to a moving reference frame, we get

$$\frac{\partial u^{*\prime}}{dr^{*\prime}} + \frac{u^{*\prime}}{r^{*\prime}} + \frac{\partial w^{*\prime}}{\partial z'} = 0 \tag{8}$$

$$\mu\nabla^2 \left[1 - \frac{1}{\bar{\alpha}^2} \nabla^2 \right] w^{*\prime} = \frac{dp'}{dz'} + \rho^* g\beta^* (T' - T_0') + \rho^* g\beta^* (C' - C_0') + \frac{sin\emptyset}{F} + \delta_1 {B_0}^2 w^{*\prime} + \frac{\mu}{k} w^{*\prime} \tag{9}$$

$$\left[u^{*\prime} \frac{\partial T'}{\partial r^{*\prime}} + w^{*\prime} \frac{\partial T'}{\partial z'} \right] = \beta^* \left[\frac{\partial^2 T'}{\partial {r^{*\prime}}^2} + \frac{1}{r^{*\prime}} \frac{\partial T'}{\partial r^{*\prime}} + \frac{\partial^2 T'}{\partial {z'}^2} \right] + \tau \left\{ D_B{}^* \left[\frac{\partial C'}{\partial r^{*\prime}} \frac{\partial T'}{\partial r^{*\prime}} + \frac{\partial C'}{\partial z'} \frac{\partial T'}{\partial z'} \right] + \frac{D_{T'}{}^*}{T_0'} \left[\left(\frac{\partial T'}{\partial r^{*\prime}} \right)^2 + \left(\frac{\partial T'}{\partial z'} \right)^2 \right] \right\} \tag{10}$$

$$\left[u^{*\prime} \frac{\partial C'}{\partial r^{*\prime}} + w^{*\prime} \frac{\partial C'}{\partial z'} \right] = D_B{}^* \left[\frac{\partial^2 C'}{\partial {r^{*\prime}}^2} + \frac{1}{r^{*\prime}} \frac{\partial C'}{\partial r^{*\prime}} + \frac{\partial^2 C'}{\partial {z'}^2} \right] + \frac{D_{T'}{}^*}{T_0'} \left[\frac{\partial^2 T'}{\partial {r^{*\prime}}^2} + \frac{1}{r^{*\prime}} \frac{\partial T'}{\partial r^{*\prime}} + \frac{\partial^2 T'}{\partial {z'}^2} \right] \tag{11}$$

with $\nabla^2 = \frac{1}{r^*} \frac{\partial}{\partial r^*} \left(r^* \frac{\partial}{\partial r^*} \right)$

where $\tau = \frac{(\rho^* C)_p}{(\rho^* C)_f}$ and $F = \frac{1}{\rho^* g}$

The dimensionless quantities:

$$r^* = \frac{r^{*\prime}}{a^*}, h' = \frac{h}{a^*}, z = \frac{z'}{\lambda^*}, w^* = \frac{w^{*\prime}}{c_1}, p = \frac{{a^*}^2 p'}{\lambda^* c_1 \mu}, t^* = \frac{c_1 t^{*\prime}}{\lambda^*}, u^* = \frac{\lambda u^{*\prime}}{a^* c_1}, \theta^* = \frac{T' - T_0'}{T_0'},$$

$$R_e = \frac{2\rho^* c_1 a^*}{\mu},\ \beta^* = \frac{k_1}{(\rho^* C)_f}, N_b^* = \frac{(\rho^* C)_p D_B{}^* C_0'}{(\rho^* C)_f}, N_t^* = \frac{(\rho^* C)_p D_{T'}{}^* T_0'}{(\rho^* C)_f \beta^*}, \sigma^* = \frac{C' - C_0'}{C_0'},$$

$$\bar{\alpha} = a^* \emptyset = \sqrt{\frac{\mu}{\eta}} a^*,\ k = \frac{k}{{a^*}^2}, M^* = \frac{\delta_1 {B_0}^2 {a^*}^2}{\mu}, G_r^* = \frac{g\beta^* {a^*}^3 T_0'}{\gamma^2}, B_r^* = \frac{g\beta^* {a^*}^3 C_0'}{\gamma^2}$$

Here G_r^* and B_r^* are the temperature and nanoparticle Grashof numbers, respectively. They quantify the ratio of buoyancy forces to the viscous forces in the flow. A larger B_r^* signifies a stronger influence of free convection induced by nanoparticle concentration differences.

Substituting the dimensionless quantities into equations (8) to (11), and taking long wavelength and low Reynolds number approximations while omitting the initial terms, we get

$$\frac{\partial p}{\partial r} = 0 \tag{12}$$

$$\frac{1}{r^*} \frac{\partial}{\partial r^*} \left(r^* \frac{\partial}{\partial r^*} \left(1 - \frac{1}{\bar{\alpha}^2} \nabla^2 \right) w^* \right) = \frac{dp}{dz} + G_r^* \theta^* + B_r^* \sigma^* + \frac{sin\emptyset}{F} + \left(\frac{\mu}{k} + M^* \right) w^* \tag{13}$$

$$0 = \frac{1}{r^*} \frac{\partial}{\partial r^*} \left(r^* \frac{\partial \theta^*}{\partial r^*} \right) + N_b^* \frac{\partial \sigma^*}{\partial r^*} \frac{\partial \theta^*}{\partial r^*} + N_t^* \left(\frac{\partial \theta^*}{\partial r^*} \right)^2 \tag{14}$$

$$0 = \frac{1}{r^*} \frac{\partial}{\partial r^*} \left(r^* \frac{\partial \sigma^*}{\partial r^*} \right) + \frac{N_t^*}{N_b^*} \left(\frac{1}{r^*} \frac{\partial}{\partial r^*} \left(r^* \frac{\partial \theta^*}{\partial r^*} \right) \right) \tag{15}$$

Dimensionless boundary conditions are

$$\frac{\partial w^*}{\partial r^*} = 0, \frac{\partial \sigma^*}{\partial r^*} = 0, \frac{\partial \theta^*}{\partial r^*} = 0 \text{ at } r^* = 0 \tag{16}$$

$$w^* = 0, \sigma^* = 0, \theta^* = 0 \text{ at } r^* = h(z) = 1 + \epsilon sin 2\pi z \tag{17}$$

$$\frac{\partial^2 w^*}{\partial r^{*2}} - \frac{\overline{\eta}}{r^*}\frac{\partial w^*}{\partial r^*} = 0 \text{ at } r^* = h(z) = 1 + \epsilon sin2\pi z \tag{18}$$

$$\frac{\partial^2 w^*}{\partial r^{*2}} - \frac{\overline{\eta}}{r^*}\frac{\partial w^*}{\partial r^*} \text{ is finite at } r^* = 0 \tag{19}$$

Here $\epsilon^* = \frac{b^*}{a^*}$ and $\eta' = \frac{\overline{\eta}}{\eta}$

SOLUTION OF THE PROBLEM

HPM: It combines the perturbation and homotopy methods. This methodology is more suitable than the other classic perturbation approaches.

The homotopy formulations for (14) and (15) are (He, J. H. (1999))

$$H(\varsigma, \theta^*) = (1-\varsigma)[L(\theta^*) - L(\theta_{10}^*)] + \varsigma\left[N_b^*\left(\frac{\partial \sigma^*}{\partial r^*}\right)\left(\frac{\partial \theta^*}{\partial r^*}\right) + N_t^*\left(\frac{\partial \theta^*}{\partial r^*}\right)^2\right] \tag{20}$$

$$H(\varsigma, \sigma^*) = (1-\varsigma)[L(\sigma^*) - L(\sigma_{10}^*)] + \varsigma\left[\frac{N_t^*}{N_b^*}\left(\frac{1}{r^*}\frac{\partial}{\partial r^*}\left(r^*\frac{\partial \theta^*}{\partial r^*}\right)\right)\right] \tag{21}$$

Let the linear operator be $L = \frac{1}{r^*}\frac{\partial}{\partial r^*}\left(r^*\frac{\partial}{\partial r^*}\right)$ and

$\theta_{10}^*(r^*, z) = \left(\frac{r^{*2}-h^2}{4}\right), \sigma_{10}^*(r^*, z) = -\left(\frac{r^{*2}-h^2}{4}\right)$ are initial guesses (22)

Define

$$\theta^*(r^*, z) = \theta_0^* + \varsigma\theta_1^* + \varsigma^2\theta_2^* + ------ \tag{23}$$

$$\sigma^*(r^*, z) = \sigma_0^* + \varsigma\sigma_1^* + \varsigma^2\sigma_2^* + ------ \tag{24}$$

Expressions for nanoparticle concentration and temperature profile are obtained for $\varsigma = 1$ as

$$\sigma^* = -\frac{N_t^*}{N_b^*}(N_b^* - N_t^*)\left(\frac{r^{*4}-h^4}{64}\right) \tag{25}$$

$$\theta^* = N_b^*(N_b^* - N_t^*)\left(\frac{r^{*6}-h^6}{1152}\right) - 2N_t^*(N_b^* - N_t^*)\left(\frac{r^{*6}-h^6}{1152}\right) + (2N_t^* - N_b^*)\left(\frac{r^{*4}-h^4}{64}\right) \tag{26}$$

Substituting (25) and (26) in equation (13), we get

$$\frac{1}{r^*}\frac{\partial}{\partial r^*}\left(r^*\frac{\partial}{\partial r^*}\left(1 - \frac{1}{\bar{\alpha}^2}\nabla^2\right)w^*\right) = \frac{dp}{dz} + \frac{sin\phi}{F} + G_r^*\left[N_b^*(N_b^* - N_t^*)\left(\frac{r^{*6}-h^6}{1152}\right) - 2N_t^*(N_b^* - N_t^*)\left(\frac{r^{*6}-h^6}{1152}\right) + (2N_t^* - N_b^*)\left(\frac{r^{*4}-h^4}{64}\right)\right] + B_r^*\left(-\frac{N_t^*}{N_b^*}(N_b^* - N_t^*)\left(\frac{r^{*4}-h^4}{64}\right)\right) + \left(\frac{\mu}{k} + M^*\right)w^* \tag{27}$$

On solving equation (27) using the boundary conditions, we get

$$w^* = \frac{1}{\left[1-\bar{\alpha}^2\left(\frac{r^{*2}}{4} - \left(\frac{\mu}{k}+M^*\right)\frac{r^4}{64}\right)\right]}\bar{\alpha}^2\left\{\left(\frac{dp}{dz} + \frac{sin\emptyset}{F}\right)\left(-\frac{r^{*4}}{64} + \frac{h^2 r^{*2}}{16} - \frac{3h^4}{64}\right) - G_r^*\left[N_b^*(N_b^* - N_t^*)\left(\frac{r^{*10}}{7372800} - \frac{h^6 r^{*4}}{73728} + \frac{5h^8 r^{*2}}{98304} - \frac{23h^{10}}{614400}\right) - N_t^*(N_b^* - N_t^*)\left(\frac{r^{*10}}{3686400} - \frac{h^6 r^{*4}}{36864} + \frac{5h^8 r^{*2}}{50752} - 0.00000716628h^{10}\right) + (2N_t^* - N_b^*)\left(\frac{r^{*8}}{147456} - \frac{h^4 r^{*4}}{4096} + \frac{h^6 r^{*2}}{1152} - \frac{31h^8}{49152}\right)\right] - B_r^*\left[-\frac{N_t^*}{N_b^*}(N_b^* - N_t^*)\left(\frac{r^{*8}}{147456} - \frac{h^4 r^{*4}}{4096} + \frac{h^6 r^{*2}}{1152} - \frac{31h^8}{49152}\right)\right]\right\} \tag{28}$$

Dimensionless flux is

$$q^* = \int_0^h 2r^* w^* dr^* \tag{29}$$

Substituting w^* from (28) in (29) and solving, we get

$$q^* = \bar{\alpha}^2\left\{\left(\frac{dp}{dz}+\frac{sin\emptyset}{F}\right)\left[-\frac{h^6}{48}+\bar{\alpha}^2\left(-\frac{5h^8}{3072}-\left(\frac{\mu}{k}+M^*\right)\left(\frac{-h^{10}}{20480}\right)\right)\right]-G_r^*\left[N_b^*(N_b^*-N_t^*)\left(-\frac{73h^{12}}{4423680}+\bar{\alpha}^2\left(-0.000001283676h^{14}-\left(\frac{\mu}{k}+M^*\right)(-0.00000003841188h^{16})\right)\right)-N_t^*(N_b^*-N_t^*)\left(0.0000330958h^{12}+\bar{\alpha}^2\left(0.0000056283h^{14}-\left(\frac{\mu}{k}+M^*\right)(0.00000377848h^{16})\right)\right)+(2N_t^*-N_b^*)\left(-\frac{17h^{10}}{61440}+\bar{\alpha}^2\left(-\frac{19h^{12}}{884736}-\left(\frac{\mu}{k}+M^*\right)(-0.00000064184h^{14})\right)\right)\right]-B_r^*\left[-\frac{N_t^*}{N_b^*}(N_b^*-N_t^*)\left(-\frac{17h^{10}}{61440}+\bar{\alpha}^2\left(-\frac{19h^{12}}{884736}-\left(\frac{\mu}{k}+M^*\right)(-0.00000064184h^{14})\right)\right)\right]\right\} \quad (30)$$

From equation (30), the expression for $\frac{dp}{dz}$ is

$$\frac{dp}{dz} = -\frac{1}{A_1}q^* + \frac{B_1}{A_1} \quad (31)$$

Where $A_1 = \bar{\alpha}^2\left[-\frac{h^6}{48}+\bar{\alpha}^2\left(-\frac{5h^8}{3072}+\left(\frac{\mu}{k}+M^*\right)\frac{h^{10}}{20480}\right)\right]$
and

$$B_1 = \bar{\alpha}^2\left\{\frac{sin\emptyset}{F}\left[-\frac{h^6}{48}+\bar{\alpha}^2\left(-\frac{5h^8}{3072}+\left(\frac{\mu}{k}+M^*\right)\left(\frac{h^{10}}{20480}\right)\right)\right]-G_r^*\left[N_b^*(N_b^*-N_t^*)\left(-\frac{73h^{12}}{4423680}+\bar{\alpha}^2\left(-0.00000128h^{14}+\left(\frac{\mu}{k}+M^*\right)(0.0000000384h^{16})\right)\right)-N_t^*(N_b^*-N_t^*)\left(0.000033h^{12}+\bar{\alpha}^2\left(0.0000056h^{14}-\left(\frac{\mu}{k}+M^*\right)(0.00000378h^{16})\right)\right)+(2N_t^*-N_b^*)\left(-\frac{17h^{10}}{61440}+\bar{\alpha}^2\left(-\frac{19h^{12}}{884736}+\left(\frac{\mu}{k}+M^*\right)(0.00000064184h^{14})\right)\right)\right]-B_r^*\left[-\frac{N_t^*}{N_b^*}(N_b^*-N_t^*)\left(-\frac{17h^{10}}{61440}+\bar{\alpha}^2\left(-\frac{19h^{12}}{884736}+\left(\frac{\mu}{k}+M^*\right)(0.00000064184h^{14})\right)\right)\right]\right\}$$

Pressure drop over the wavelength is

$$\Delta p_\lambda{}^* = -\int_0^1 \frac{dp}{dz}dz \quad (32)$$

By substituting $\frac{dp}{dz}$ from (31) in (32), we get

$$\Delta p_\lambda{}^* = q^*S_1 + S_2 \quad (33)$$

$$\text{Here } S_1 = -\int_0^1 \frac{1}{A_1}dz \quad (34)$$

and

$$S_2 = \int_0^1 \frac{B_1}{A_1}dz \quad (35)$$

Time-averaged flux is

$$Q^* = 1 + \frac{\epsilon^{*2}}{2} + q^* \quad (36)$$

By substituting (33) in (36), time-averaged flux is

$$Q^* = 1 + \frac{\epsilon^{*2}}{2} + \frac{\Delta p_\lambda{}^*}{S_1} - \frac{S_2}{S_1} \quad (37)$$

The dimensionless frictional force is given as

$$F^* = \int_0^1 h^2 \left(-\frac{dp}{dz}\right) dz \tag{38}$$

Mechanical efficiency is defined as $E^* = \frac{\text{useful pumping power}}{\text{total work done per wavelength}}$

$$E^* = \frac{\Delta p_\lambda{}^* Q^*}{\frac{3b^{*2}}{8}\Delta p_\lambda{}^* + \int_0^1 \int_0^1 \frac{dp}{dz}\{b^* sin2\pi(z-t^*) - b^{*2} sin^4\pi(z-t^*) dz dt^*\}} \tag{39}$$

Maximum flow rate is

$$Q_0{}^* = 1 + \frac{\epsilon^{*2}}{2} + \frac{\int_0^1 \frac{B_1}{A_1} dz}{\int_0^1 \frac{1}{A_1} dz} \tag{40}$$

The reflux limit is

$$Q^* < 1 + \frac{\epsilon^{*2}}{2} + \frac{\int_0^1 \frac{B_1}{A_1} dz}{\int_0^1 \frac{1}{A_1} dz} \tag{41}$$

Graphical Illustrations

Semi analytical approaches are used to obtain expressions of concentration, temperature, reflux limit, mechanical efficiency, frictional force, pressure drop, velocity, and time-averaged flux. Figures in the following subsections display graphical findings of relevant parameters for σ^*, θ^*, E^*, $\Delta p_\lambda{}^*$, $F^*$and reflux limit by using Mathematica.

Pressure drop

Figure (2) illustrates variation of absolute value of pressure drop for different values of $G_r{}^*, B_r{}^*, N_b{}^*, \mu,\ N_t{}^*, M^*, k^*$ compared to time-averaged flux (Q^*). Figures 2(a)-2(g) shows that rise in porosity (k), and Brownian motion parameter ($N_b{}^*$) results in an undesirable reaction in pressure drop ($\Delta p_\lambda{}^*$), whereas $\Delta p_\lambda{}^*$ rises with larger magnitudes of magnetic parameter (M^*), nanoparticle Grashof number ($B_r{}^*$), thermophoresis parameter ($N_t{}^*$), temperature Grashof number ($G_r{}^*$), and dynamic viscosity (μ).

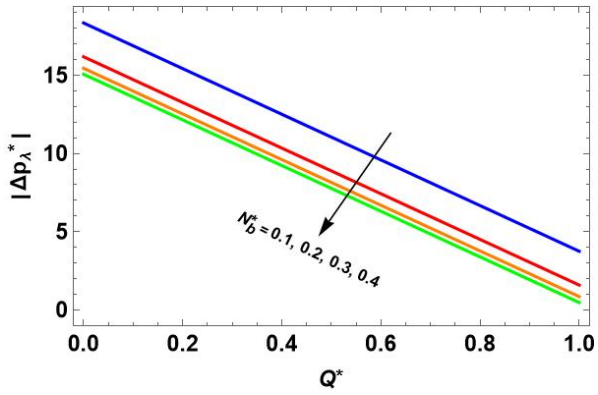

Figure 2(a). Variations in Pressure drop for $N_b{}^*$

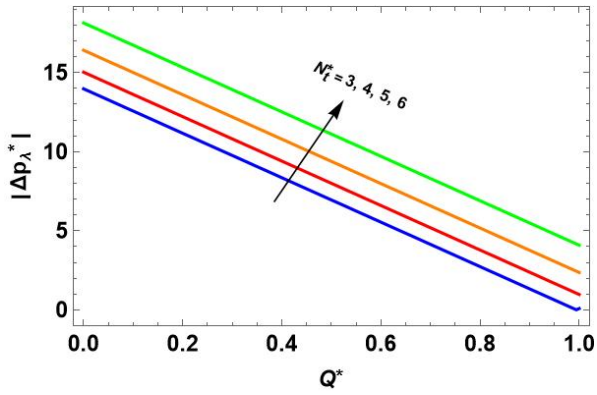

Figure 2(b). Variations in Pressure drop for $N_t{}^*$

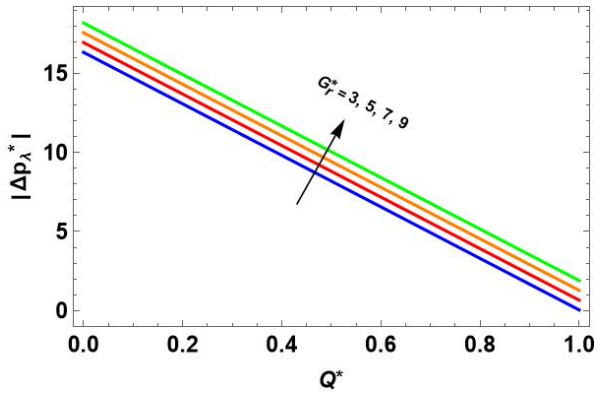

Figure 2(c). Variations in Pressure drop for $G_r{}^*$

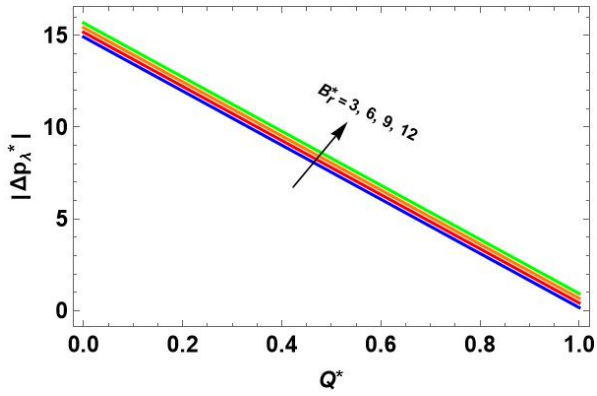

Figure 2(d). Variations in Pressure drop for $B_r{}^*$

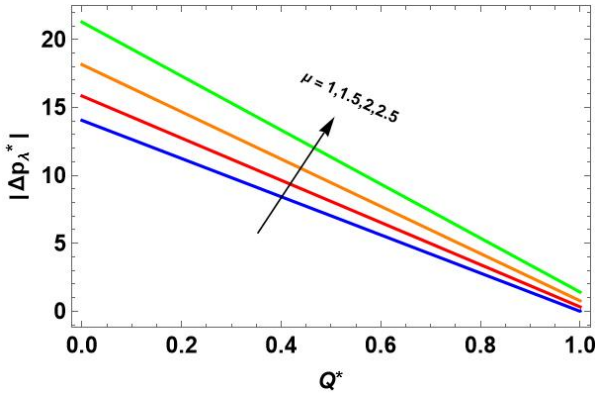

Figure 2(e). Variations in Pressure drop for μ

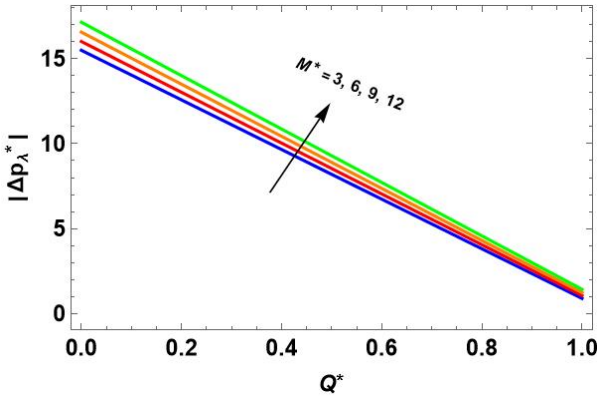

Figure 2(f). Variations in Pressure drop for M^*

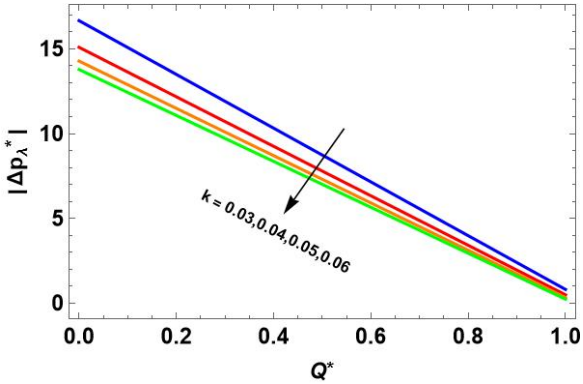

Figure 2(g). Variations in Pressure drop for k

Frictional Force

Figure 3(a)-3(g) shows how various parameters affect the frictional force (F^*). F^* upsurges with rise in thermophoresis ($N_t{}^*$), temperature Grashof number ($G_r{}^*$), nanoparticle Grashof number ($B_r{}^*$), dynamic viscosity (μ), magnetic parameter (M^*) but decreases with rise in porosity (k), and Brownian motion ($N_b{}^*$).

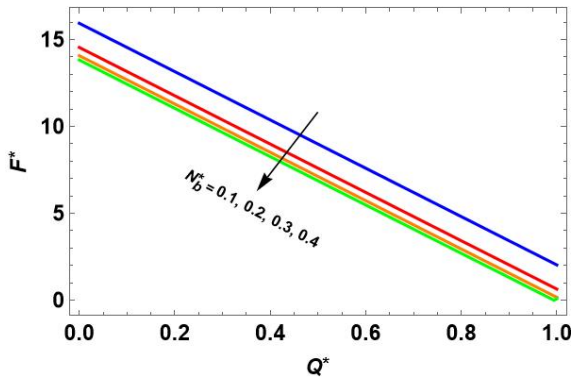

Figure 3(a). Variations in Frictional force F^* against $N_b{}^*$

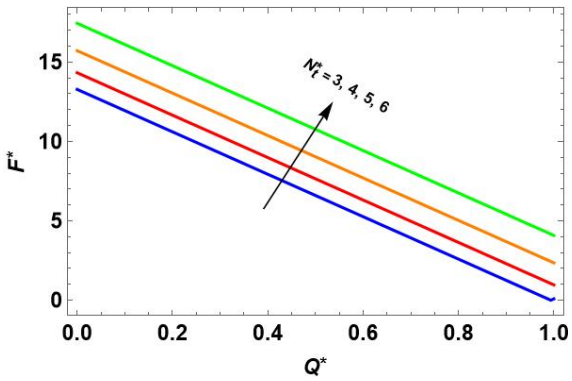

Figure 3(b). Variations in Frictional force F^* against $N_t{}^*$

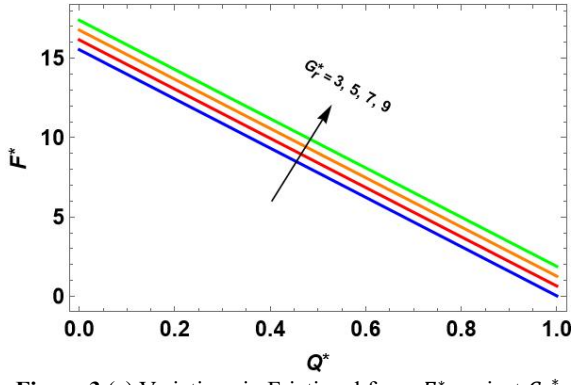

Figure 3 (c) Variations in Frictional force F^* against $G_r{}^*$

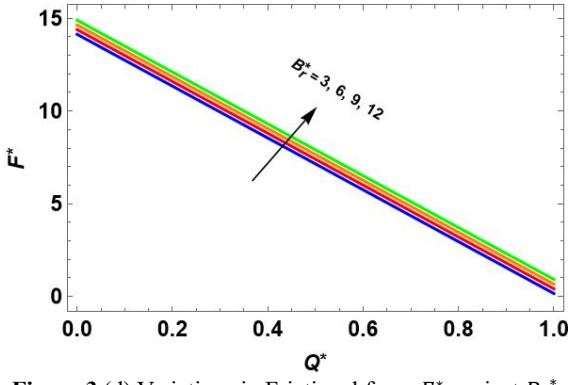

Figure 3 (d) Variations in Frictional force F^* against $B_r{}^*$

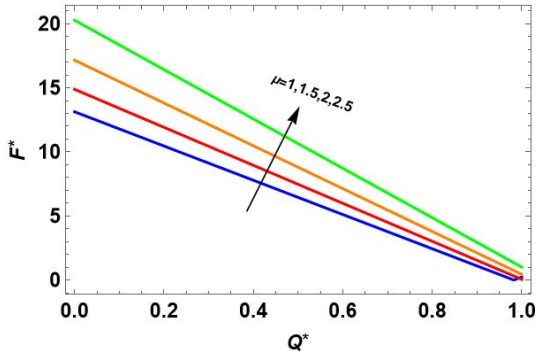

Figure 3(e). Variations in Frictional force F^* against μ

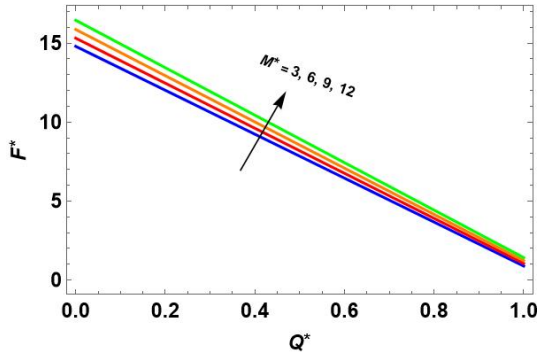

Figure 3(f). Variations in Frictional force F^* against M^*

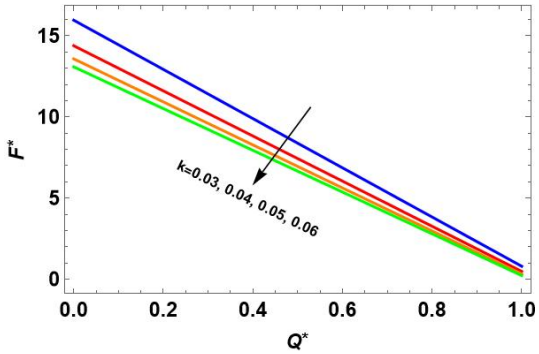

Figure 3(g). Variations in Frictional force F^* against k

Temperature Profile

Figure (4) illustrates the variations of temperature (θ^*) for thermophoresis ($N_t{}^*$) and Brownian motion ($N_b{}^*$). Decrease in $N_t{}^*$ and $N_b{}^*$ causes a rise in temperature, which signifies the enhanced thermal diffusion resulting from intensified nanoparticle motion, which acts to homogenize the temperature field.

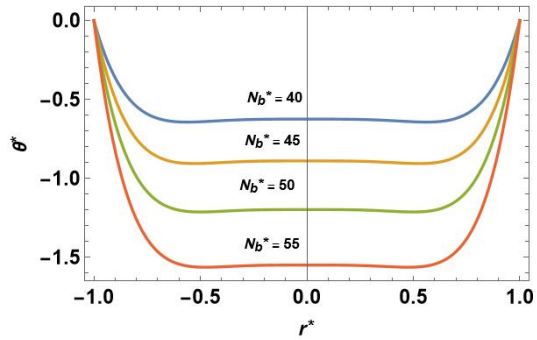

Figure 4(a). Effect of $N_b{}^*$ on Temperature

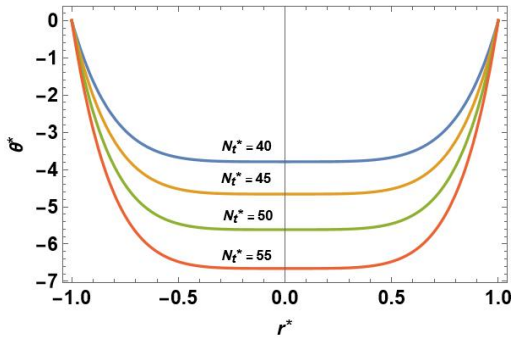

Figure 4(b). Effect of $N_t{}^*$ on Temperature

Nanoparticle Phenomena

Figure (5) shows that increasing the Brownian motion ($N_b{}^*$) improves concentration, but increasing thermophoretic parameter ($N_t{}^*$) decreases concentration significantly.

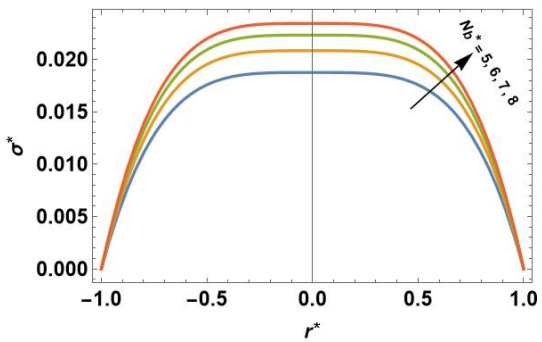

Figure 5(a) Nanoparticle phenomenon against $N_b{}^*$

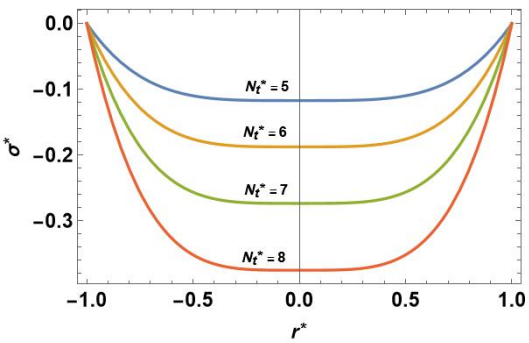

Figure 5(b) Nanoparticle phenomenon against $N_t{}^*$

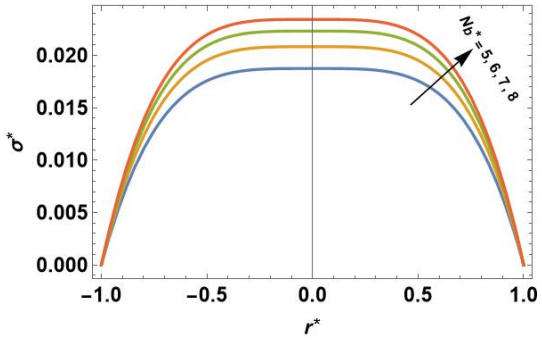

Figure 5(a) Nanoparticle phenomenon against $N_b{}^*$

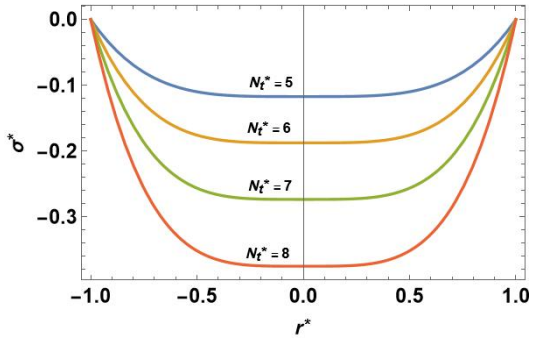

Figure 5(b) Nanoparticle phenomenon against $N_t{}^*$

Mechanical Efficiency

Figure (6 and 6.1), Variations in Mechanical efficiency E^* are illustrated for different values of $\mu, N_b{}^*, k, N_t{}^*, G_r{}^*, M^*, B_r{}^*$ compared to amplitude (b^*) and the ratio of averaged flow rate and maximum flow rate $(Q^*/Q_0{}^*)$. Figures 6(a)-6(g), shows that rise in porosity k, nanoparticle Grashof number $B_r{}^*$, and Brownian motion N_b^* results in an undesirable reaction in Mechanical efficiency(E^*) whereas E^* rises with larger magnitudes of magnetic parameter (M^*), temperature Grashof number $(G_r{}^*)$, dynamic viscosity (μ), and thermophoresis parameter $(N_t{}^*)$. Figures 6.1(a)-(g), show that E^* upsurges with rise in nanoparticle Grashof number $B_r{}^*$, porosity k, and Brownian motion N_b^* whereas E^* reduces with increase in dynamic viscosity (μ), temperature Grashof number $G_r{}^*$, thermophoresis parameter $(N_t{}^*)$, and magnetic parameter (M^*).

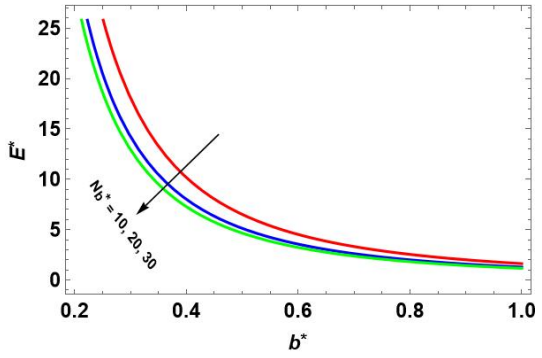

Figure 6(a). Mechanical Efficiency vs amplitude for different $N_b{}^*$

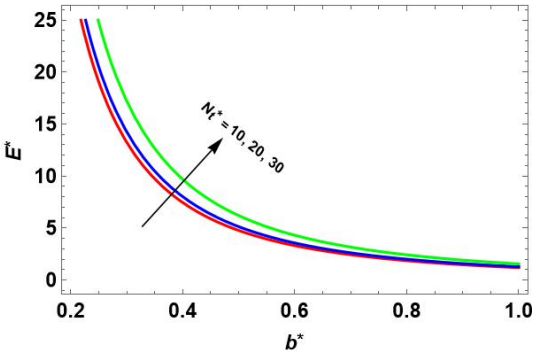

Figure 6(b). Mechanical Efficiency vs amplitude for different $N_t{}^*$

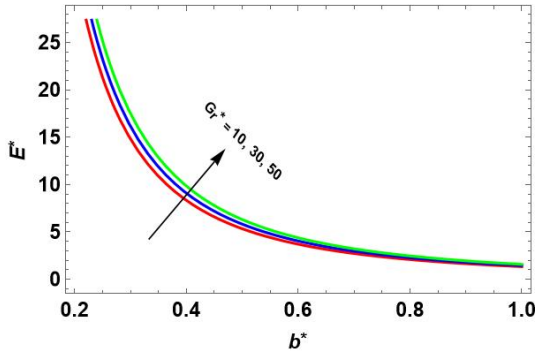

Figure 6(c). Mechanical Efficiency vs amplitude for different $G_r{}^*$

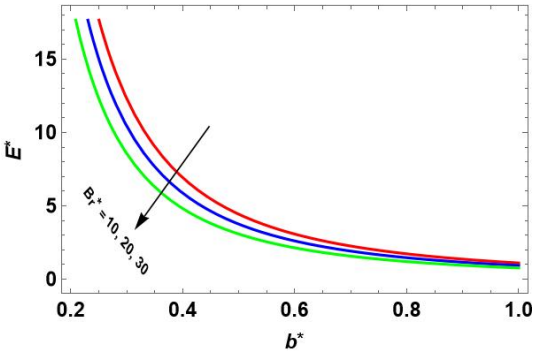

Figure 6(d). Mechanical Efficiency vs amplitude for different $B_r{}^*$

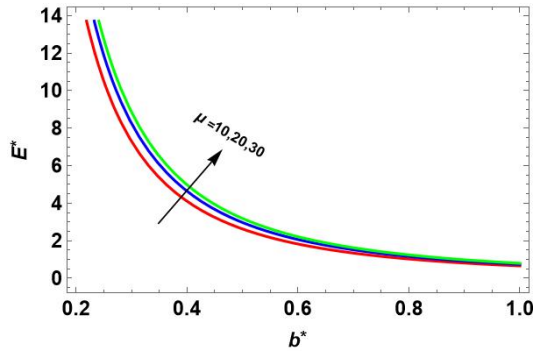

Figure 6(e). Mechanical Efficiency vs amplitude for different μ

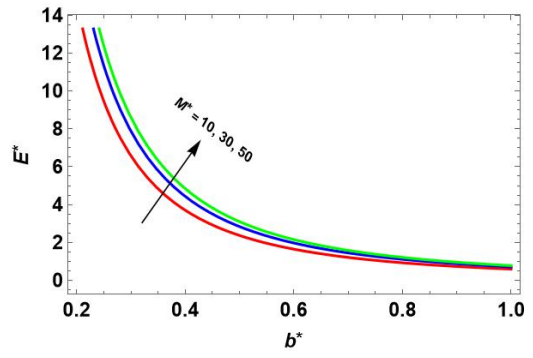

Figure 6(f). Mechanical Efficiency vs amplitude for different M^*

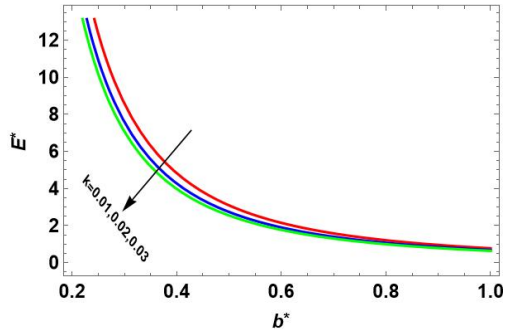

Figure 6(g). Mechanical Efficiency vs amplitude for different k

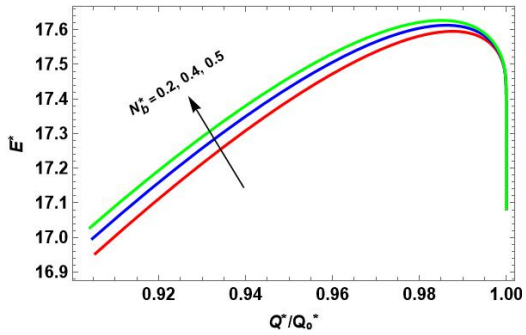

Figure 6.1(a). Mechanical Efficiency vs $Q^*/{Q_0}^*$ for different ${N_b}^*$

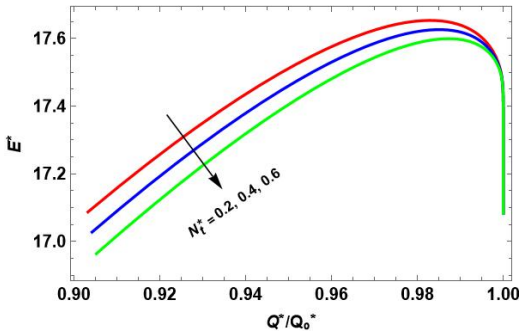

Figure 6.1(b). Mechanical Efficiency vs $Q^*/{Q_0}^*$ for different ${N_t}^*$

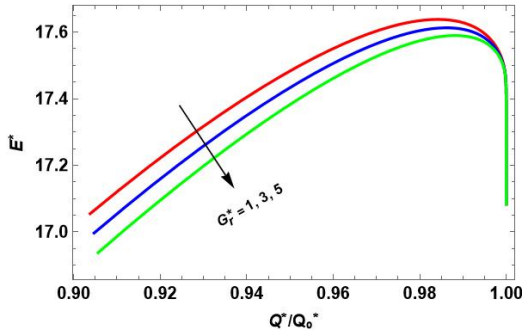

Figure 6.1(c). Mechanical Efficiency vs $Q^*/{Q_0}^*$ for different ${G_r}^*$

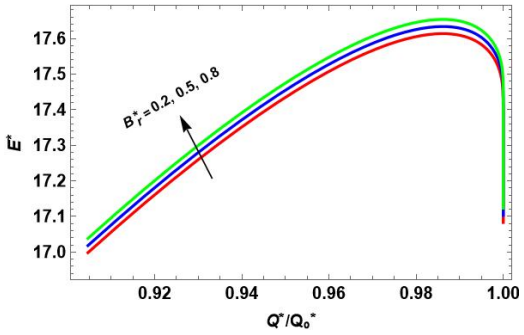

Figure 6.1(d). Mechanical Efficiency vs $Q^*/{Q_0}^*$ for different ${B_r}^*$

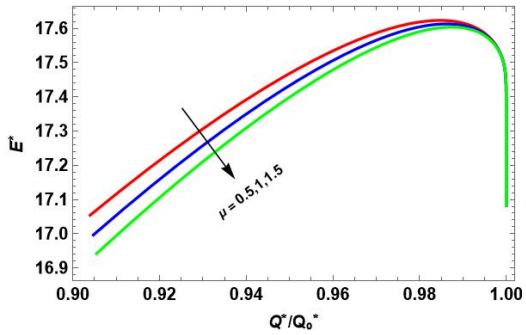

Figure 6.1(e). Mechanical Efficiency vs $Q^*/{Q_0}^*$ for different μ

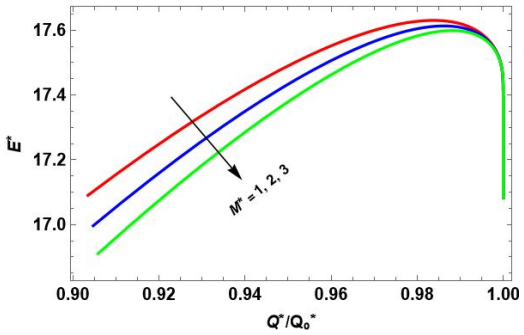

Figure 6.1(f). Mechanical Efficiency vs $Q^*/{Q_0}^*$ for different M^*

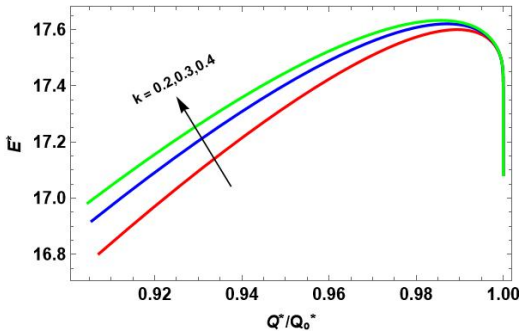

Figure 6.1(g). Mechanical Efficiency vs $Q^*/{Q_0}^*$ for different k

Reflux Limit

Figure 7(a)-7(g) show that, with increase in nanoparticle Grashof number B_r^*, porosity k, temperature Grashof number G_r^*, and thermophoresis N_t^* results in a significant increase in reflux flow rate whereas higher values of magnetic parameter M^*, Brownian motion N_b^* and dynamic viscosity μ results in a reduction in reflux flow rate.

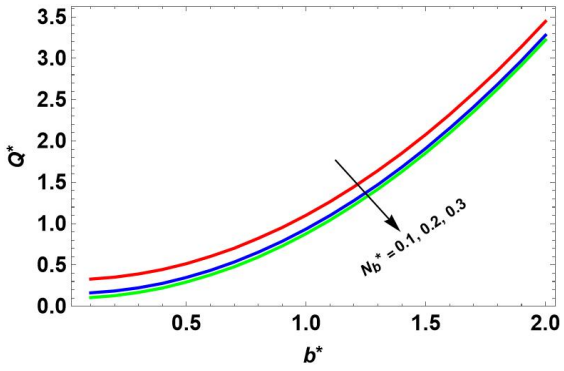

Figure 7(a). Reflux limit against $N_b{}^*$

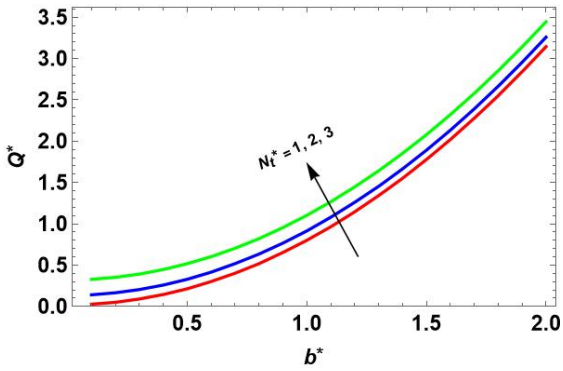

Figure 7(b). Reflux limit against $N_t{}^*$

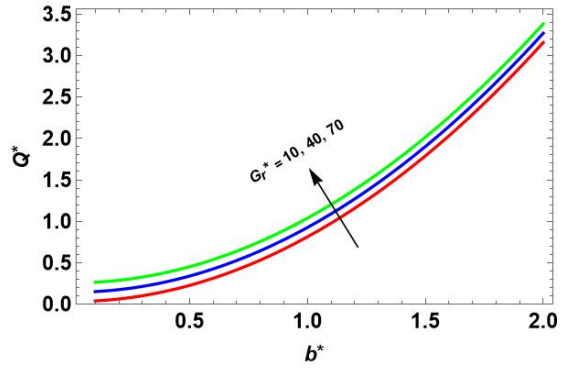

Figure 7(c). Reflux limit against $G_r{}^*$

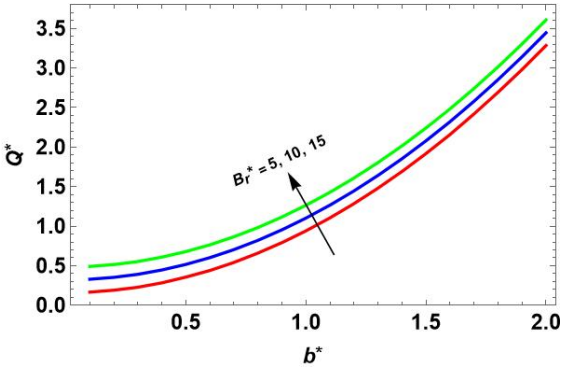

Figure 7(d). Reflux limit against $B_r{}^*$

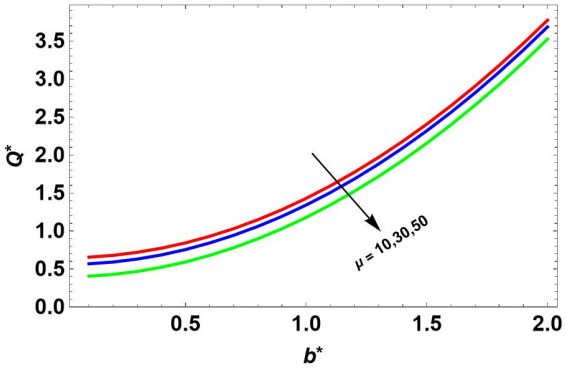

Figure 7(e). Reflux limit against μ

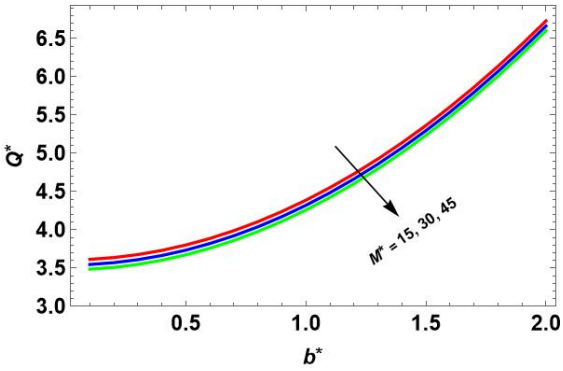

Figure 7(f). Reflux limit against M^*

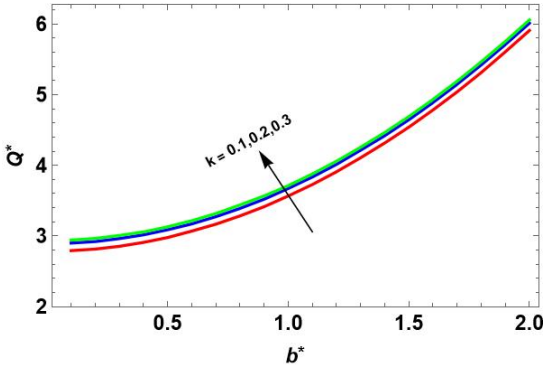

Figure 7(g). Reflux limit against k

Comparing the result with previous study

Magnetohydrodynamic effects on the peristaltic flow of couple stress fluid in an inclined tube with endoscope (previous study)	**Impact of Magnetic field on peristaltic transport of Nano-coupled stress fluid in an inclined porous tube (present study)**
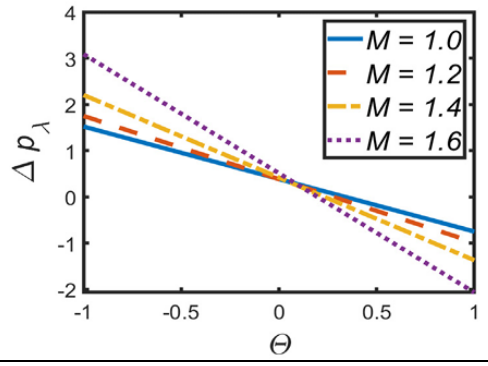	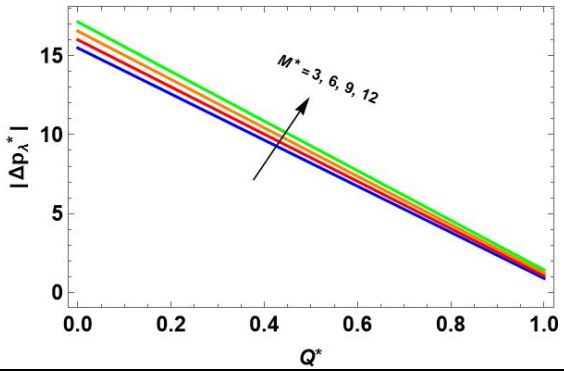
Variations in Pressure drop for M	Variations in Pressure drop for M^*

CONCLUSIONS

Governing equations for an incompressible nano-coupled stress fluid passing through a circular tube under the influence of magnetic field in porous medium are modeled and used to simulate fluid flow in the tube. The study under consideration is crucial from a rheological standpoint, and it has applications in various scientific fields, including fluid flow simulation. This research focuses on how nanoparticle Grashof number (${B_r}^*$), porous medium (k^*), magnetic parameter (M^*), and temperature Grashof number (${G_r}^*$) affect net flow rate. The key conclusions of the present research are:

- Thermophoresis (N_t^*) and Brownian motion (N_b^*) decreases as temperature upsurges.
- Increase in Brownian motion parameter N_b^*, increases concentration whereas it reduces with rise in thermophoresis N_t^*.
- Decrease in porous medium parameter (k^*) and Brownian motion (N_b^*) increases pressure-drop, but increasing thermophoresis (${N_t}^*$) and magnetic parameter (M^*) significantly increases pressure drop.
- Frictional force (F^*) upsurges as magnetic parameter (M^*) and thermophoretic parameter (N_t^*) increases, whereas F^* reduces with rise in porous medium parameter (k^*) and Brownian motion (N_b^*).
- An elevation in the thermophoresis parameter N_t^*, nanoparticle Grashof number ${B_r}^*$, porosity k, and temperature Grashof number G_r^* substantially augments the reflux flow rate which promote fluid movement by enhancing thermal convection, reducing viscous drag, and allowing freer passage through the porous medium. Elevated values of μ, M^*, and N_b^* leads to decrease in reflux limit.
- An increase in B_r^*, N_b^*, and k leads to decrease in mechanical efficiency. This behavior suggests that enhanced nanoparticle diffusion, elevated viscous dissipation, and increased permeability introduce greater resistance and energy loss within the system. Conversely, higher values of the temperature Grashof number (G_r^*), thermophoresis parameter (N_t^*), dynamic viscosity (μ), and magnetic parameter (M^*) are associated with an improvement in mechanical efficiency. These parameters appear to promote more stable and directed fluid motion, potentially due to stronger thermal gradients, buoyancy effects, and controlled stress fields that enhance flow alignment.
- Interestingly, mechanical efficiency E^* expressed exclusively in terms of the flow rate ratio (${Q^*/Q_0}^*$) reveals an opposite trend in certain cases i.e., increasing N_b^*, B_r^*, and k results in enhanced mechanical efficiency and in contrast, larger values of N_t^*, G_r^*, μ and M^* lead to a decrease in mechanical efficiency under the same flow conditions. This indicates that, depending on the operating regime, excessive thermophoretic effects, strong magnetic field interactions may suppress efficient energy transport within the system. Changing porosity or nanoparticle Grashof number can change time-averaged flow by affecting buoyancy-driven convection and also change frictional dissipation by adjusting viscosity. If the modification increases flux more than dissipation then E^* increases otherwise it reduces.
- When $N_b^* = 0, N_t^* = 0, M^* = 0, k = 0$, the velocity or pressure relations can be reduced to long wavelength solution. Increasing the MHD parameter (M^*) reduces reflux and stabilizes pumping. Moderate levels of the thermophoresis parameter (N_t^*) implies good nanoparticle distribution while preventing excessive energy loss. The inclination angle can be optimized to reduce reflux in biomedical devices or systems.

ORCID

M.P. Molimol, https://orcid.org/0000-0001-5343-9138; **K. Maruthi Prasad,** https://orcid.org/0000-0002-9010-6452;
N. Subadra, https://orcid.org/0000-0001-8901-1870

REFERENCES

[1] P. Deepalakshmi, G. Shankar, E.P. Siva, D. Tripathi, and O. Anwar Beg, "MHD Analysis of Couple Stress Nanofluid through a Tapered Non-Uniform Channel with Porous Media and Slip-Convective Boundary Effects", International Journal of Thermofluids, **27**, 101208 (2025). https://doi.org/10.1016/j.ijft.2025.101208

[2] M.M. Ahmed, I.M. Eldesoky, Ahmed G. Nasr, Ramzy M. Abumandour, and Sara I. Abdelsalam, "The profound effect of heat transfer on magnetic peristaltic flow of a couple stress fluid in an inclined annular tube", Modern Physica Letter B, **38**(25), No. 25, 2450233 (2024). https://doi.org/10.1142/S0217984924502336

[3] M. Devakar, K. Ramesh, and K. Vajravelu, "Magnetohydrodynamic effects on the peristaltic flow of couple stress fluid in an inclined tube with endoscope", Journal of Computational Mathematics and Data Science, **2**, 2772-4158 (2022). https://doi.org/10.1016/j.jcmds.2022.100025

[4] A.H. Shapiro, M.Y. Jaffrin, and S.L. Weinberg, "Peristaltic pumping with long wavelengths at low Reynolds number", Journal of Fluid Mechanics, **37**(04), 799–825 (1969). https://doi.org/10.1017/s0022112069000899

[5] K.M. Prasad, N. Subadra, and U.S. Mahabaleshwar, "Peristaltic Transport of a Couple-Stress Fluid with Nanoparticles in an Inclined Tube", International Journal of Engineering Trends and Technology (IJETT), **48**(7), 354-362 (2017). https://doi.org/10.14445/22315381/IJETT-V48P262

[6] V.K. Stokes, "Couple stresses in fluids", Physics of Fluids, **9**(9), 1709–1715 (1966). https://doi.org/10.1063/1.1761925

[7] D. Pal, N. Rudraiah, and R. Devanathan, "A couple stress model of blood flow in the microcirculation", Bulletin of Mathematical Biology, **50**(4), 329–344 (1988). https://doi.org/10.1007/BF02459703

[8] S. Maiti, and J. Misra, "Peristaltic transport of a couple stress fluid: some applications to hemodynamics", Journal of Mechanics in Medicine and Biology, **12**(03), 1250048 (2012). https://doi.org/10.1142/S0219519411004733

[9] K.M. Prasad, and G. Radhakrishnamacharya, "Effect of Peripheral Layer on Peristaltic Transport of a Couple Stress Fluid", International Journal of Fluid Mechanics Research, **36**(6), 573–583 (2009). https://doi.org/10.1615/InterJFluidMechRes.v36.i6.80

[10] G.C. Shit, and M. Roy, "Hydromagnetic effect on inclined peristaltic flow of a couple stress fluid", Alexandria Engineering Journal, **53**(4), 949–958 (2014). https://doi.org/10.1016/j.aej.2014.07.007

[11] S.U.S. Choi, and J.A. Eastman, "Enhancing thermal conductivity of fluids with nanoparticles", in: *ASME FED, Proceedings of the ASME International Mechanical Engineering Congress and Exposition*, (San Francisco, CA, 1995).

[12] K.M. Prasad, N. Subadra, and M. Srinivas, "Peristaltic Transport of a Nanofluid in an Inclined Tube", American Journal of Computational and Applied Mathematics, **5**(4), 117–128 (2015). https://doi.org/10.5923/j.ajcam.20150504.04
S.K. Das, N. Putra, and W. Roetzel, "Pool boiling of nano-fluids on horizontal narrow tubes", International Journal of Multiphase Flow, **29**(8), 1237-1247 (2003). https://doi.org/10.1016/S0301-9322(03)00105-8

[13] S. Noreen, "Mixed Convection Peristaltic Flow of Third Order Nanofluid with an Induced Magnetic Field", PLoS ONE, **8**(11), e78770 (2013). https://doi.org/10.1371/journal.pone.0078770

[14] K.M. Prasad, N. Subadra, and M. Srinivas "Study of Peristaltic Motion of Nano Particles of a Micropolar Fluid with Heat and Mass Transfer Effect in an Inclined Tube", in: *International conference on computational heat and mass transfer (ICCHMT) - 2015*, **127**, 694–702 (2015). https://doi.org/10.1016/j.proeng.2015.11.368

[15] N.S. Akbar, and S. Nadeem, "Peristaltic flow of a micropolar fluid with nanoparticles in small intestine", Applied Nanoscience, **3**(6), 461-468 (2013). https://doi.org/10.1007/s13204-012-0160-2

[16] D. Srinivasacharya, M. Mishra, and A.R. Rao, "Peristaltic pumping of a micropolar fluid in a tube" Acta Mechanica, **161**(3-4), 165–178 (2003). https://doi.org/10.1007/s00707-002-0993-y

[17] A.E.H.A.El. Naby, and I.El. Shamy, "Slip effects on peristaltic transport of power-law fluid through an inclined tube", Applied Mathematical Sciences, **1**(60), 2967–2980 (2007).

[18] K. Maruthi Prasad, and G. Radhakrishnamacharya, "Flow of Herschel–Bulkley fluid through an inclined tube of non-uniform cross-section with multiple stenoses", Archives of Mechanics, **60**(2), 161–172 (2008).

ВПЛИВ МАГНІТНОГО ПОЛЯ НА ПЕРИСТАЛЬТИЧНИЙ ТРАНСПОРТ НАНОРІДИНИ З НАПРУЖЕННЯМИ У ПОХИЛІЙ ПОРИСТІЙ ТРУБЦІ

М.П. Молімол[1,2], К. Маруті Прасад[1], Н. Субадра[2]

[1]Кафедра математики, школа природничих наук, GITAM (Вважається університетом), Хайдерабад, Телангана, Індія -502329
[2]Кафедра математики, інженерно-технологічний коледж Гітанджалі, Район Медчал, Хайдерабад, Телангана, Індія -501301

Це дослідження пропонує теоретичне дослідження перистальтичного транспорту нанорідини з напруженнями під впливом магнітного поля в похилій пористій трубці. З низьким числом Рейнольдса, наближеннями довгих хвиль, використовуються відповідні аналітичні методи для дослідження швидкості рідини, сили тертя, усередненого за часом потоку, явищ наночастинок, перепаду тиску та профілю температури. Досліджено вплив різних фізичних параметрів, включаючи параметр термофорезу, параметр броунівського руху, локальне число Грасгофа для наночастинок та локальне число Грасгофа для температури, на характеристики сили тертя та перепаду тиску. Графіки використовуються для ілюстрації виразів для перепаду тиску, швидкості, явищ, пов'язаних з наночастинками, температурного профілю та сили тертя.

Ключові слова: *параметр термофорезу; перистальтика; параметр броунівського руху; наночастинки; магнітне поле; рідина з парним напруженням; пористе середовище*